THE JOURNAL OF PHYSICAL CHEMISTRY C

Article

Cite This: J. Phys. Chem. C 2019, 123, 26351−26357

pubs.acs.org/JPCC

Structural and Physical Parameters Controlling the Oxygen Reduction Reaction Selectivity with Carboxylic Acid-Substituted Cobalt Corroles Incorporated in a Porous Carbon Support

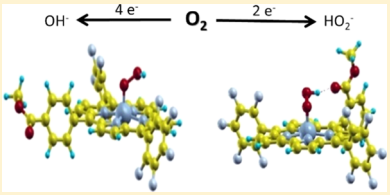
Hilah C. Honig,[†] Chethana B. Krishnamurthy,[†,§] Ignacio Borge-Durán,[†,§] Mariusz Tasior,[‡,§] Daniel T. Gryko,*[,‡] Ilya Grinberg,*[,†] and Lior Elbaz*[,†]

[†]Department of Chemistry, Bar-Ilan University, Ramat-Gan 5290002, Israel

[‡]Institute of Organic Chemistry, Polish Academy of Sciences, Kasprzaka 44-52, 01-224 Warsaw, Poland

Supporting Information

ABSTRACT: Three cobalt(III) complexes of regioisomeric *trans*-A_2B-corroles were designed and efficiently synthesized. The corroles were adsorbed on smooth glassy carbon (GC) and black pearls 2000 (BP2000), high-surface-area carbon. Albeit spatially separated from the cobalt reaction center, the position of COOH group has a profound influence on the oxygen reduction reaction electrocatalytic reactivity when on GC, whereas on BP2000, a significant increase in selectivity toward the 4-electron reduction was observed in an alkaline environment. This is attributed to the wetting properties of the hydrophobic pores of BP2000, which considerably lower the dielectric constant in the pore water environment, stabilize the charged OOH^- intermediate, and favor the 4-electron reduction pathway with the cobalt-bis-pentafluorophenyl (phenyl-*para*-carboxylic acid), when compared to analogous corroles with the COOH group at the ortho- and meta-positions.



INTRODUCTION

The oxygen reduction reaction (ORR) is one of the most important processes in nature. It is also utilized, among many other applications, for the generation of electricity in fuel cells. Platinum has traditionally been used as an electrocatalyst for ORR in low-temperature fuel cells,[1] while this reaction is still considered to be the limiting factor for the overall performance of the cell.[2] To obtain high power density, large quantity of platinum is used.[3] The scarcity of Pt and its derived price are considered the main obstacles for large-scale commercialization of low-temperature fuel cells.[4,5]

To overcome this hurdle, the development of a platinum group metal-free (PGM-free) catalyst is necessary, as was recently highlighted by the U.S. DOE Fuel Cells Technologies Office.[6]

In 1964, Jasinski reported the first ORR catalysts based on the earth-abundant organo-metallic macrocyclic structure containing a cobalt complex, cobalt phthalocyanine.[7] Over the last several decades, a great deal of research has been done with cobalt and iron−N_4 macrocyclic complexes, which mimic the activity of the corrin and its analogues in vitamin B_{12}.[8−10] One of the challenges in such catalyst design is to mimic the electron/proton transfer interplay that is carried out very efficiently in enzymes.[11,12]

In this regard, modified metallo-corroles have been receiving increased attention. Corrole is a tetrapyrrolic macrocyclic compound that acts as a trianionic ligand, unlike corrins and porphyrins, which are mono- and dianionic ligands, respectively. The particular ligand behavior of corrole is of interest because of its potential electrocatalytic activity.[13,14] These compounds have shown to be versatile ligands that can coordinate transition metals without significant distortion of the macrocycle plane.[15]

Previously published theoretical and experimental studies show that of Mn, Fe, Co, Ni, and Cu, cobalt is the most active metal center for ORR with metallo-corroles, in terms of both reaction overpotential and selectivity.[16−19] In addition, the effect of various electron-withdrawing substituents on the corrole β- and meso-positions was studied and optimized to reduce the ORR overpotential, achieving the state-of-the-art activity for a PGM-free molecular (non-heat-treated) ORR catalyst.[16,20,21]

Herein, we report the synthesis, ORR electrocatalytic activity,[22] and density functional theory (DFT) calculations[23] of three different cobalt(III) triphenylcorrolates, which contain electron-withdrawing, proton-donating substituents at the meso positions. The structures of the compounds studied in this work are shown in Figure 1 and denoted here as *ortho*-corrole, *meta*-corrole, and *para*-corrole. They possess two stabilizing C_6F_5 groups at positions 5 and 15 and a C_6H_4COOH group at position 10. They differ in the location of carboxylic group versus linkage to the corrole core.

EXPERIMENTAL SECTION

Synthesis. *10-[3-(Methoxycarbonyl)phenyl]-5,15-bis-(pentafluorophenyl)corrole (**6**).* Pentafluorophenyldi-pyrrane

Received: August 1, 2019
Revised: October 3, 2019
Published: October 9, 2019

Downloaded via BAR-ILAN UNIV on March 24, 2020 at 09:43:23 (UTC).
See https://pubs.acs.org/sharingguidelines for options on how to legitimately share published articles.

© 2019 American Chemical Society

DOI: 10.1021/acs.jpcc.9b07333
J. Phys. Chem. C 2019, 123, 26351−26357

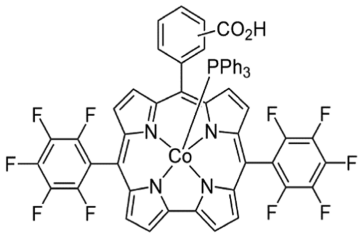


Figure 1. Structures of cobalt(III) corrolates possessing the COOH group at three different positions (ortho, meta, and para).

(**1**) (780 mg, 2.5 mmol) and 3-(methoxycarbonyl)-benzaldehyde (**3**) (205 mg, 1.25 mmol) were dissolved in MeOH (125 mL). Concentrated HCl(aq) (6.25 mL) in water (125 mL) was then added, and the resulting suspension was stirred at room temperature for 1.5 h. The reaction mixture was extracted with $CHCl_3$ (2 × 50 mL), and the organic phase was washed with water (3 × 50 mL), dried (Na_2SO_4), and concentrated to 20 mL volume. Dichlorodicyanoquinone (735 mg, 3.25 mmol) was dissolved in toluene/CH_2Cl_2 (1:1, 20 mL), and both mixtures were added simultaneously, via syringes, to the vigorously stirred CH_2Cl_2 (50 mL). After 15 min, the reaction mixture was concentrated to one-fourth of the initial volume and filtered through a silica pad (CH_2Cl_2). The red fluorescent band was collected, evaporated, and chromatographed (silica, CH_2Cl_2/hexanes, 3:2). The corrole fraction was collected, evaporated, and crystallized from $CHCl_3$/hexanes to afford pure corrole (560 mg, 59%) as dark violet crystals. Mp 281−282 °C. ^{1}H NMR (500 MHz, $CDCl_3$) δ 9.12 (br s, 2H, β-H), 8.83 (br s, 1H, Ar), 8.73 (br d, J = 4.2 Hz, 2H, β-H), 8.63 (br d, J = 4.2 Hz, 2H, β-H), 8.58 (br s, 2H, β-H), 8.43 (d, J = 7.4 Hz, 1H, Ar), 8.36 (d, J = 4.5 Hz, 1H, Ar), 7.85 (t, J = 7.2 Hz, 1H, Ar), 3.96 (s, 3H, CO_2CH_3), −2.50 (br s, 3H, inner NH); HRMS (ESI) [M + H$^+$] calcd: 765.1348 for $C_{39}H_{19}N_4O_2F_{10}$, observed 765.1339; λ_{abs} (toluene, $\varepsilon \times 10^{-3}$, M^{-1} cm^{-1}) 423 (121), 563 (19.2), 615 (11.3), 638 (7.66) nm.

ortho-Corrole. Corrole **5** has been obtained following the literature protocol.[24] Corrole **5** (95 mg, 0.125 mmol) was dissolved in 15 mL of tetrahydrofuran (THF) and 7.5 mL of MeOH. KOH (200 mg, 3.57 mmol, 30 equiv) in water (4 mL) was added, and the resulting mixture was stirred at reflux for 3 h under a nitrogen atmosphere. After cooling down, acetic acid (0.75 mL) was added and the reaction mixture was concentrated and partitioned between water and dichloromethane. The organic phase was separated, and the aqueous phase was extracted few times with dichloromethane until it was no longer violet. The combined organic extracts were washed with brine, dried under Na_2SO_4, and evaporated, to afford crude carboxylic acid (CA), which was used in the next step without any further purification. Alternatively, carboxylic acid is obtained from corrole **5** by hydrolysis under acidic conditions, as described for *para*-corrole. Crude carboxylic acid prepared in the first step (94 mg, 0.125 mmol) was dissolved in the mixture of MeOH (35 mL) and THF (15 mL). Then, NaOAc (150 mg, 1.83 mmol) was added, and the resulting mixture was stirred for 5 min at room temperature. PPh_3 (250 mg, 0.95 mmol) was added, followed by $Co(OAc)_2{\cdot}4H_2O$ (150 mg, 0.6 mmol). The reaction mixture was stirred at room temperature for 16 h, evaporated, and chromatographed (silica, toluene/acetone, 95:5). The corrole fraction was collected, evaporated, and crystallized from $CHCl_3$/hexanes to afford pure *ortho*-corrole (88 mg, 66%) as red crystals. The compound being the product of substitution of one fluorine atom with a methoxy group was also isolated and identified on the basis of ESI-MS. Mp > 350 °C. ^{1}H NMR (mixture of two atropoisomers in 2:1 ratio) (500 MHz, $CDCl_3$) δ 8.68 (d, J = 4.4 Hz, 0.66H, β-H), 8.48 (d, J = 4.4 Hz, 1.33H, β-H), 8.22 (d, J = 4.0 Hz, 1.33H, β-H), 8.17 (d, J = 4.8 Hz, 2H, β-H), 8.09 (d, J = 6.2 Hz, 0.66H, Ar), 8.04 (d, J = 4.9 Hz, 0.66H, β-H), 7.99 (d, J = 4.0 Hz, 0.66H, β-H), 7.95 (d, J = 4.4 Hz, 1.33H, β-H), 7.89−7.87 (m, 0.66H, Ar), 7.73−7.69 (m, 2H, Ar), 7.64 (td, J = 7.5, 1.2 Hz, 0.33H, Ar), 7.20 (d, J = 7.4 Hz, 0.33H, Ar), 7.04−6.99 (m, 3H, Ph), 6.69−6.64 (m, 6H, Ph), 4.75−4.70 (m, 4H, Ph), 4.65−4.60 (m, 2H, Ph); HRMS (ESI) [M + H$^+$] calcd: 1068.1122 for $C_{56}H_{28}N_4O_2F_{10}PCo$, observed 1068.1107; λ_{abs} (toluene, $\varepsilon \times 10^{-3}$, M^{-1} cm^{-1}) 381 (42.6), 412 (44.0), 559 (10.8) nm.

meta-Corrole. Corrole **6** (180 mg, 0.23 mmol) was dissolved in 15 mL of THF and 7.5 mL of MeOH. KOH (400 mg, 7.14 mmol, 30 equiv) in water (4 mL) was added, and the resulting mixture was stirred at reflux for 3 h under a nitrogen atmosphere. After cooling down, acetic acid (1.5 mL) was added and the reaction mixture was concentrated and partitioned between water and dichloromethane. The organic phase was separated, and the aqueous phase was extracted few times with dichloromethane until it was no longer violet. The combined organic extracts were washed with brine, dried under Na_2SO_4, and evaporated, to afford crude carboxylic acid, which was used in the next step without any further purification. Alternatively, carboxylic acid is obtained from corrole **6** by hydrolysis under acidic conditions, as described for *para*-corrole. Crude carboxylic acid prepared in the first step (180 mg, 0.25 mmol) was dissolved in the mixture of MeOH (70 mL) and THF (30 mL). Then, NaOAc (320 mg, 3.66 mmol) was added, and the resulting mixture was stirred for 5 min at room temperature. PPh_3 (500 mg, 1.9 mmol) was added, followed by $Co(OAc)_2{\cdot}4H_2O$ (300 mg, 1.2 mmol). The reaction mixture was stirred at room temperature for 16 h, evaporated, and chromatographed (silica, toluene/acetone, 95:5). The corrole fraction was collected, evaporated, and crystallized from $CHCl_3$/hexanes to afford pure *meta*-corrole (176 mg, 72%) as a red amorphous solid. The compound being the product of substitution of one fluorine atom with a methoxy group was also isolated and identified on the basis of ESI-MS. ^{1}H NMR (mixture of two atropoisomers in 1:0.8 ratio) (500 MHz, $CDCl_3$) δ 8.71 (d, J = 4.4 Hz, 1.1H, β-H), 8.67 (d, J = 4.6 Hz, 0.9H, β-H), 8.38−8.34 (m, 0.9H, Ar), 8.19 (d, J = 4.2 Hz, 2.2H, β-H), 8.15 (d, J = 4.8 Hz, 0.9H, β-H), 8.12−8.09 (m, 2H, β-H + Ar), 7.99−7.95 (m, 2H, β-H), 7.71−7.58 (m, 2H, Ar), 6.99−6.95 (m, 3H, Ph), 6.63−6.59 (m, 6H, Ph), 4.65−4.60 (m, 6H, Ph); HRMS (ESI) [M + H$^+$] calcd: 1068.1122 for $C_{56}H_{28}N_4O_2F_{10}PCo$, observed 1068.1145; λ_{abs} (toluene, $\varepsilon \times 10^{-3}$, M^{-1} cm^{-1}) 382 (45.2), 410 (44.1), 559 (10.3), 590 (8.3) nm.

para-Corrole. Corrole **7** (382 mg, 0.5 mmol) was dissolved in the mixture of AcOH (9 mL), TFA (4.5 mL), and 5% aq H_2SO_4 (3 mL). The green solution was protected from light and stirred at 100 °C under an argon atmosphere. The reaction progress was monitored on thin-layer chromatography (TLC). After 48 h, all ester was consumed (only start spot on TLC), the reaction mixture was cooled down, and $NaHCO_3$ (5% aq) was carefully added. The violet solution was extracted with $CHCl_3$ (three times), dried (Na_2SO_4), evaporated, and dried under high vacuum to afford the crude acid. Crude carboxylic

DOI: 10.1021/acs.jpcc.9b07333
J. Phys. Chem. C 2019, 123, 26351−26357

acid prepared in the first step (57 mg, 0.075 mmol) was dissolved in EtOH (15 mL). NaOAc (90 mg, 1.1 mmol) was added and, the resulting mixture was stirred for 5 min at room temperature. PPh_3 (150 mg, 0.57 mmol) was added, followed by $Co(OAc)_2{\cdot}4H_2O$ (90 mg, 0.36 mmol). The reaction mixture was stirred at room temperature for 16 h, evaporated, and chromatographed (silica, CH_2Cl_2/MeOH, 98:2). The corrole fraction was collected, evaporated, and crystallized from hexanes to afford pure *para*-corrole (71 mg, 89%) as violet crystals. ^{1}H NMR (500 MHz, $CDCl_3$) δ 8.76 (d, J = 4.4 Hz, 2H, β-H), 8.43, (d, J = 8.0 Hz, 1H, C_6H_4), 8.37 (d, J = 8.0 Hz, 1H, C_6H_4), 8.28 (d, J = 4.8 Hz, 2H, β-H), 8.26 (d, J = 4.8 Hz, 2H, β-H), 8.21 (d, J = 8.0 Hz, 1H, C_6H_4), 8.05 (d, J = 4.4 Hz, 2H, β-H), 7.56 (d, J = 8.0 Hz, 1H, C_6H_4), 7.07−7.03 (m, 3H, Ph), 6.71−6.67 (m, 6H, Ph), 4.65−4.60 (m, 6H, Ph); HRMS (ESI) [M + H$^+$] calcd: 1068.1122 for $C_{56}H_{28}N_4O_2F_{10}PCo$, observed 1068.1119; λ_{abs} (toluene, $\varepsilon \times 10^{-3}$, M^{-1} cm^{-1}) 383 (33.9), 412 (33.9), 558 (7.31), 590 (6.00) nm.

Electrochemical Measurements. Rotating ring-disk electrode (RRDE) (glassy electrode disc surface of 0.2475 cm^2, and a platinum ring) measurements were conducted using a Biologic VSP potentiostat and a Pine rotator. A glassy carbon rod and a reversible hydrogen electrode (RHE) were used as the counter and reference electrodes, respectively. All measurements were conducted in 0.1 M aqueous solution of KOH (Acros, 98%). Background currents were measured after purging Ar (Maxima, 99.99%) into the cell and were subtracted from the results. When testing the catalytic performance of the system toward ORR, pure O_2 (99.99%) was purged into the cell for 20 min prior to the measurement and during the measurement to assure the saturation of the solution with dissolved oxygen.

For all electrode preparations, the catalyst ink was prepared by dissolving 0.2 mg of corrole in 1 mL of isopropanol.[25] In previous studies, it was shown that the activity of metallo-corroles can be significantly increased, when they are adsorbed on high-surface-area carbon supports, such as black pearls 2000 (BP2000). To achieve high ORR activity and to enable the study of the effect of the substituent on it, the metallo-corroles studied here were adsorbed on BP2000. To do so, 10 mg of BP2000 carbon and 0.8 mg of corrole were mixed in 1 mL of isopropanol and stirred overnight to allow the corrole to adsorb onto the carbon surface, according to a procedure described elsewhere.[25] The samples were then centrifuged and the carbon was separated from the excess corrole and solvent. Then, 1 mL of solution containing 2:1 (volumetric ratio) of isopropanol/deionized water and 0.2 wt % Nafion was added to the carbon−corrole composite. The catalyst slurry (10 μL) was applied on the glassy carbon surface of a rotating ring-disk electrode and was left to dry at room temperature. This method of electrode preparation was used for all of the corroles studied in this work.

Modeling. The structural optimization and total energy calculation were performed using the density functional theory (DFT) method as implemented in the Quantum ESPRESSO package.[26] The exchange−correlation energy of the electrons was represented by the Perdew−Burke−Ernzerhof functional within the generalized gradient approximation.[27,28] The valence and core electron interactions were described by pseudopotential from the GBRV database.[29] The Kohn−Sham orbitals were expanded using a plane-wave basis set up to 50 Ry energy cutoff, and the Brilliouin zone was sampled only at the γ point. The Methfessel−Paxton smearing method was employed with the smearing parameter of 0.01 Ry.[30] Geometry optimizations were carried out with the converge threshold of 10^{-3} and 10^{-5} Ry for the total energy and the force on each atom, respectively.

The binding energies (ΔE) of the adsorbate intermediates in the ORR pathway[31] were calculated using the following equations

$$\Delta E_O = (E_{\text{corrole}-O} + E_{H_2}) - (E_{H_2O} + E_{\text{bare corrole}})$$

$$\Delta E_{OH} = \left(E_{\text{corrole}-OH} + \frac{1}{2}E_{H_2}\right) - (E_{H_2O} + E_{\text{bare corrole}})$$

$$\Delta E_{OOH} = \left(E_{\text{corrole}-OOH} + \frac{3}{2}E_{H_2}\right) - (2E_{H_2O} + E_{\text{bare corrole}})$$

We have carried out the calculation of the bare corroles and the corroles with adsorbed OH, O, and OOH for both singlet and triplet spin states. We find that the triplet state is preferred for the bare corrole and the corrole-O, while the singlet state is preferred for corrole-OH and corrole-OH, and the binding energies given in Table 3 are calculated using the lower-energy spin state for each molecule. We also find that similar differences in ΔE_O, ΔE_{OH}, and ΔE_{OOOH} between the *ortho*- and *para*-corroles and the much higher ΔE_O for the corrole than for Pt(111) are obtained regardless of the choice of the spin state.

RESULTS AND DISCUSSION

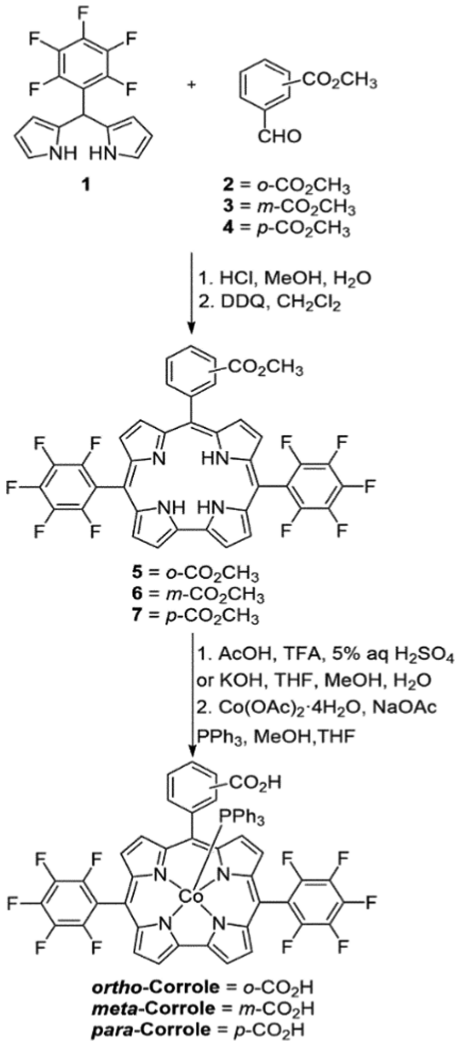
Synthesis. The synthesis of the cobalt corroles was achieved in 2−3 steps as described on Scheme 1. First, pentafluorophenyldipyrrane (**1**) was condensed with methyl *o*-, *m*-, or *p*-formylbenzoates **2**−**4**, respectively, under the conditions optimized by Gryko and Koszarna.[32] Then, the resulting ester corroles **5**−**7** were subjected to hydrolysis. It was found that hydrolysis under acidic conditions generally gives good results; however, it requires long reaction times to achieve satisfying conversion rates and sometimes leads to a large number of side-products. Therefore, ester hydrolysis of corroles **5** and **6** was conducted under basic conditions using KOH in the MeOH/THF/H_2O mixture. This results in much faster conversion; however, formation of significant amounts of side-products was observed, which after ESI-MS analysis were identified as a product of substitution of one or two fluorine atoms with methoxy groups. Nevertheless, crude carboxylic acids obtained by both methods were subjected to the metallation reaction under typical conditions (cobalt(II) acetate, sodium acetate in MeOH/THF mixture), which after chromatographic purification yielded desired complexes *ortho*-corrole, *meta*-corrole, and *para*-corrole, in good overall yield.

In general, ORR can follow one of three possible mechanisms: the most desired (1) direct 4-electron reduction to water, (2) 2 + 2-electron reduction going through the less-desired peroxide intermediate, and the least desired (3) 2-electron reduction, producing peroxide, which is considered detrimental to the catalyst and the cell, in addition to lowering the overall currents and thus the overall power density. Hence, controlling the selectivity of the reaction through the design of the catalytic center and its surroundings is of critical importance.

Electrocatalysis. Metallo-corroles are considered among the state-of-the-art molecular ORR catalysts in terms of

DOI: 10.1021/acs.jpcc.9b07333
J. Phys. Chem. C 2019, 123, 26351−26357

Scheme 1. Synthesis of Studied Cobalt Corroles



reactivity (kinetics and potential). In this work, we studied the effect of the position of the carboxylic acid substituent in the meso position of the Co(III)-corrole ring on the ORR selectivity. It is expected to donate a hanging proton, which could direct the reaction more toward the 2 + 2- and even the 4-eletron mechanism. In addition, due its electron-withdrawing nature, this substituent is expected to lower the overpotential required to execute the ORR.[21,33]

The electrocatalytic activity of all three cobalt corroles synthesized in this work was studied using the rotating ring-disk electrode (RRDE), first, when dried on the surface of glassy carbon, and later, when adsorbed on high-surface-area carbon, BP2000, deposited on GC (both on RRDE). Figure 2 shows the electrocatalytic ORR activity of all three corroles in 0.1 M KOH aqueous solution when dried on a smooth glassy carbon electrode. The onset and half-wave potentials and the number of electrons calculated using the Levich equation (from the limiting current densities at 0.4 V vs RHE) are summarized in Table 1. These results show that the lowest overpotential was measured with the *ortho*-corrole. However, the *meta*-corrole is the least active in terms of onset and half-wave potentials.

Under these conditions, all three Co-corroles reduce oxygen via the less-desired 2-electron process to a peroxide anion. This is also supported by the high peroxide anion yields calculated

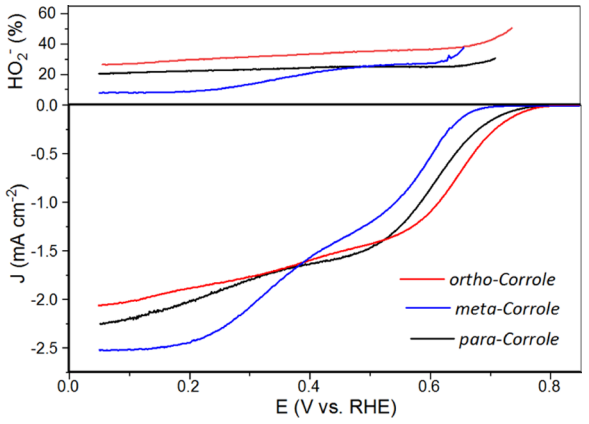


Figure 2. RRDE of the corroles dried on a GC electrode in 0.1 M KOH @ 900 rpm and 5 mV/s.

Table 1. Summary of the Potentials and Electron Numbers Obtained from the RRDE Measurements of the Corroles Dried on a GC Electrode

	E_{onset}	$E_{1/2}$	n (Levich)
ortho-corrole	0.71	0.63	2.1
meta-corrole	0.62	0.49	2.3
para-corrole	0.67	0.57	2.2

from the ring currents (Figure 2, top). The basic environment allows the carboxylic acid to deprotonate, and the substituent becomes carboxylate anion, making this substituent function as an electron donating group. In other words, the negative charge that is built in the system affects the electron transfer mechanism during the ORR process.

In previous studies, it was shown that when adsorbed in porous, high-surface-area carbon black (BP2000), metallo-corroles exhibit significantly better ORR activity due to surface interactions, which increase the electron density on the metal center and its redox potential.[21,34,35] Since this was proven to be a critical step in the formation of oxygen adduct on the catalytic site and further reduction of oxygen,[33] this procedure was repeated with the corroles studied in this work.

All three corroles showed the expected improvement in electrocatalytic activity after adsorption in BP2000, as can be seen in Figure 3 and summarized in Table 2. The overpotential of the corroles decreased by more than 130 mV when compared to the previous results on the GC electrode. Only

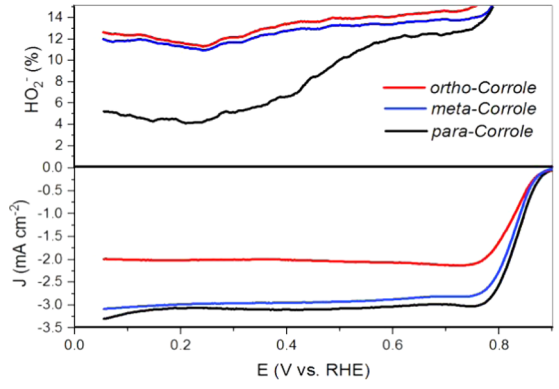


Figure 3. RRDE of the corroles adsorbed on BP2000 in 0.1 M KOH @ 900 rpm and 5 mV/s.

DOI: 10.1021/acs.jpcc.9b07333
J. Phys. Chem. C 2019, 123, 26351−26357

Table 2. Summary of the Potentials and Electron Numbers Obtained from the RRDE Measurements of the Corroles Adsorbed on BP2000

	E_{onset}	$E_{1/2}$	n (Levich)
ortho-corrole	0.86	0.82	2.0
meta-corrole	0.86	0.82	2.9
para-corrole	0.87	0.83	3.1

minor differences were measured in the onset and half-wave potentials when adsorbed in BP2000, $E_{1/2}$ = ~0.82 V vs RHE, almost independent of the position of the carboxylic acid on the phenyl ring. In contrast, the ORR mechanism seems to have improved more significantly only in the case of the *para*-corrole, for which the number of electrons calculated using the Levich equation is 3.1, getting close to the 4-electron reduction to the hydroxide anion in alkaline solution. These results are supported by the low peroxide anion yields calculated from the ring currents (as low as app. 8%, an order of magnitude lower than previously measured with GC)

To understand these results and particularly the change from the 2-electron to a 4 or 2 + 2-electron pathway observed solely for the *para*-corrole in KOH, density functional theory (DFT) calculations were carried out for the ORR pathway on the *ortho*- and *para*-corroles. These calculations show that the Co-corroles studied in this work exhibit the typical ORR pathway similar to that found in previous calculations on metallocorrole ORR catalysts.[36,37]

As observed from the data presented in Table 3, the energies of adsorbed OOH and OH intermediates relative to H_2O are

Table 3. Calculated Adsorption Energies for ORR Intermediates on CoBPF(Ph-*x*-CA)

	ortho-corrole (eV)	*para*-corrole (eV)	Pt (eV)
OOH	3.92	4.04	4.15
O	2.22	2.24	1.60
OH	0.97	1.06	0.77

slightly lower (higher) than those on the Pt(111) surface, while the energy of the adsorbed oxygen intermediate was considerably higher (by 0.6 eV) than that on Pt(111). Interestingly, variation in the position of the carboxylic acid (CA) group from para to ortho decreased the OOH and OH energies but left the oxygen energy almost unchanged. The orientation of the COOH group at the para position had no impact on the OOH and OH energies, as could be expected based on the large distance between the COOH group and the metal site of OOH and OH adsorption (Figure 4). By contrast, the binding energies of OOH and OH changed based on the relative orientation of the carbonyl. For the carbonyl oxygen pointed toward the adsorbed OOH and OH, the hydrogen bond formed between the C═O and the proton on OOH or OH lowered the energy of the adsorbate relative to the para position (Figure 4). On the other hand, for the carbonyl oxygen pointed away from the OOH and OH protons, the gas phase binding energies of OOH and OH for *ortho*-corrole were the same as for the *para*-corrole. Thus, the hydrogen bonding between the carbonyl group and the adsorbate stabilized OOH and OH relative to the *para*-corrole. As expected, the stabilization by the hydrogen bonding was greater for OOH than for OH because the larger size of OOH enabled a shorter and stronger OOH−O═C hydrogen bond.

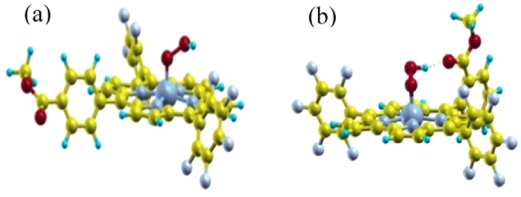


Figure 4. (a) *para*-Corrole with OOH adsorbed on the metal center and (b) *ortho*-corrole with OOH adsorbed on the metal center.

In the widely used ORR model first introduced by Nørskov and co-workers,[31] both the 2-electron and the 4-electron pathways start with the adsorption of the O_2 on the metal atom on the surface (or in corrole's case on the metal atom of the corrole), followed by the electron-coupled protonation of the O_2 and formation of OOH. The difference between the 2-electron and 4-electron pathways lies in the next step. If the metal−OOH bond is broken, the protonation results in the formation of H_2O_2 and the 2-electron pathway is obtained, while if the OOH O−O bond is broken, protonation results in the formation of H_2O, leaving an adsorbed oxygen on the surface that then continues onto the completion of the 4-electron pathway. Thus, the competition between the two pathways is governed by the energy difference between the H_2O_2 and the adsorbed O + H_2O. Since the energies of H_2O_2 and H_2O do not vary between different catalytic systems, the energy of the adsorbed oxygen atom controls the ORR pathway, with lower oxygen adsorption energy favoring the 4-electron pathway and higher adsorption energy favoring the 2-electron pathway.

Comparison of the oxygen adsorption energies on the corroles and on Pt(111) shows that the adsorbed oxygen intermediate energy is 1 eV higher for corroles than for Pt(111). This is generally the case for all molecular catalysts[37] and is likely due to the inability of the oxygen to make a full double bond with the single metal atom (Co in this case) at the active site, in contrast to the multiple Pt atoms available to create the full double bond with oxygen adsorbed on the hollow or bridge sites on the metal surfaces. The much higher energy of the oxygen adsorbate destabilizes the 4-electron pathway relative to the 2-electron pathway, leading to the production of H_2O_2 instead of two H_2O molecules.

The high energy of the oxygen intermediate explains why the 2-electron pathway is favored in acidic conditions and in basic conditions on the GC electrode for both *ortho*- and *para*-corrole because the oxygen energy of these two is essentially the same. However, it obviously cannot explain the difference observed between the *ortho*- and *para*-corrole mechanisms observed for the experiments carried out on BP2000.

We therefore attribute this difference to the difference in the solvation of OOH and HO_2^- on the BP2000 electrode in the vicinity of the *ortho*- and *para*-corrole. The corrole-filled pores of BP2000 carbon are known to be hydrophobic, making the water molecule content inside these pores considerably smaller than that in the vicinity of the surface of the glassy carbon electrode and dramatically lowering the dielectric constant of the BP2000 pore water environment.[38] In basic conditions, OOH^- is the product of the 2-electron pathway, while OH^- is the product of the 4-electron pathway. Due to their charged states, to be stable, these ions must be solvated by the water molecules.[38]

DOI: 10.1021/acs.jpcc.9b07333
J. Phys. Chem. C 2019, 123, 26351−26357

While the solvation of both of these ions can be easily achieved on glassy carbon because of the easy access of the water molecules to the corrole, the hydrophobic corrole-filled pores of BP2000 are likely to make the solvation of the OOH^- more difficult than the solvation of OH^- because the larger size of OOH^- requires additional H_2O for solvation, and only relatively few H_2O molecules are present in the BP2000 pores. This destabilizes the OOH^- product and increases the energy difference between the OOH^- product of the 2-electron pathway and the OH^- and O* products of the 4-electron pathway, favoring the 4-electron pathway for the case of the *para*-corrole. However, for the *ortho*-corrole, due to the proximity of the CA and particularly C═O carbonyl to the active site, the CA group can participate in the solvation of the OOH^- through hydrogen bonding so that fewer H_2O molecules are required for solvation of OOH^-. This stabilizes the OOH^- product of the 2-electron pathway so that this is still favored, similar to the situation for the GC electrode.

In acidic conditions, because the H_2O_2 product of the 2-electron pathway is not charged, the effect of poor solvation is much weaker[38] and the two-electron pathway is favored for both *ortho*- and *para*-corrole as is usually found for these systems (Figure 5). Thus, this work underscores the importance of considering the water environment in the vicinity of the active site and the possibility of the control of the solvation of the ORR products through the substituent groups on molecular catalysts.

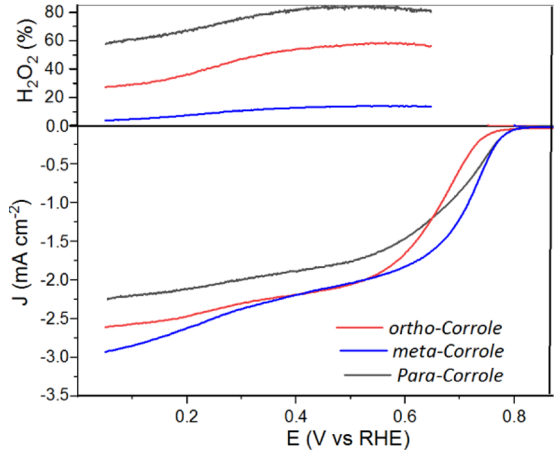


Figure 5. RRDE of the corroles when adsorbed on BP2000 in 0.5 M H_2SO_4 @ 900 rpm and 5 mV/s.

CONCLUSIONS

In this contribution, we explored the ORR on *trans*-A_2B Co-triphenyl-corrole with different positions of the carboxylic acid substituent on the meso-phenyl ring located at 10-position. It was demonstrated that these complexes on the BP2000 carbon support have different catalytic mechanisms for ORR and better ORR activity was observed for cobalt(III) corrolate catalysts on BP2000 compared to those on GC. ORR activities and the underlying mechanisms of the catalyst were characterized in detail using RRDE methods as well as a comprehensive analysis of the data. The results show that *para*-corrole incorporated in BP2000 performs an electrocatalytic reduction to oxygen with a predominantly 4-electron transfer process. DFT calculations of energetic adsorption values of the intermediates in the ORR process indicate that the difference in the mechanism is due to the difference in the solvation of the OOH^- ion in the hydrophobic low-water-content BP2000 environment. Thus, the solvation environment plays an important role in catalytic ORR and must be taken into account for the rational design of nonprecious metal catalysts.

ASSOCIATED CONTENT

Supporting Information

The Supporting Information is available free of charge on the ACS Publications website at DOI: 10.1021/acs.jpcc.9b07333.

Absorption spectra of the corroles; ^1H, ^{19}F, ^{31}P NMR spectra for synthesized compounds; and CVs of all corroles in Ar and O_2 saturated acidic and alkaline solutions (PDF)

AUTHOR INFORMATION

Corresponding Authors

*E-mail: dtgryko@icho.edu.pl (D.T.G.).
*E-mail: ilya.grinberg@biu.ac.il (I.G.).
*E-mail: lior.elbaz@biu.ac.il (L.E.).

ORCID

Chethana B. Krishnamurthy: 0000-0002-7615-5688
Daniel T. Gryko: 0000-0002-2146-1282
Lior Elbaz: 0000-0003-4989-5135

Author Contributions

§C.B.K. and I.B.-D. contributed equally.

Notes

The authors declare no competing financial interest.

ACKNOWLEDGMENTS

This work was partially supported by the Israeli Science Foundation, the Israeli Ministry of Science, and the Israeli Ministry of Energy and was conducted in the framework of the Israeli Fuel Cells Consortium (part of the Israeli National Center for Electrochemical Propulsion). This work was also supported by the National Science Centre, Poland (Grant HARMONIA 2016/22/M/ST5/00431).

REFERENCES

(1) Gasteiger, H. A.; Kocha, S. S.; Sompalli, B.; Wagner, F. T. Activity Benchmarks and Requirements for Pt, Pt-Alloy, and Non-Pt Oxygen Reduction Catalysts for PEMFCs. *Appl. Catal., B* **2005**, *56*, 9−35.

(2) Shao, Y.; Yin, G.; Gao, Y. Understanding and Approaches for the Durability Issues of Pt-Based Catalysts for Pem Fuel Cell. *J. Power Sources* **2007**, *171*, 558−566.

(3) Chen, Z.; Higgins, D.; Yu, A.; Zhang, L.; Zhang, J. A Review on Non-Precious Metal Electrocatalysts for Pem Fuel Cells. *Energy Environ. Sci.* **2011**, *4*, 3167−3192.

(4) Othman, R.; Dicks, A. L.; Zhu, Z. Non Precious Metal Catalysts for the Pem Fuel Cell Cathode. *Int. J. Hydrogen Energy* **2012**, *37*, 357−372.

(5) Shao, M.; Chang, Q.; Dodelet, J.-P.; Chenitz, R. Recent Advances in Electrocatalysts for Oxygen Reduction Reaction. *Chem. Rev.* **2016**, *116*, 3594−3657.

(6) Thompson, S. T.; James, B. D.; Huya-Kouadio, J. M.; Houchins, C.; DeSantis, D. A.; Ahluwalia, R.; Wilson, A. R.; Kleen, G.; Papageorgopoulos, D. Direct Hydrogen Fuel Cell Electric Vehicle Cost Analysis: System and High-Volume Manufacturing Description, Validation, and Outlook. *J. Power Sources* **2018**, *399*, 304−313.

(7) Jasinski, R. A New Fuel Cell Cathode Catalyst. *Nature* **1964**, *201*, 1212.

DOI: 10.1021/acs.jpcc.9b07333
J. Phys. Chem. C 2019, 123, 26351−26357

(8) Bezerra, C. W. B.; Zhang, L.; Lee, K.; Liu, H.; Marques, A. L. B.; Marques, E. P.; Wang, H.; Zhang, J. A Review of Fe−N/C and Co−N/C Catalysts for the Oxygen Reduction Reaction. *Electrochim. Acta* **2008**, *53*, 4937−4951.
(9) Rovira, C.; Kunc, K.; Hutter, J.; Parrinello, M. Structural and Electronic Properties of Co-Corrole, Co-Corrin, and Co-Porphyrin. *Inorg. Chem.* **2001**, *40*, 11−17.
(10) Wirt, M. D.; Sagi, I.; Chen, E.; Frisbie, S. M.; Lee, R.; Chance, M. R. Geometric Conformations of Intermediates of B12 Catalysis by X-Ray Edge Spectroscopy: Cobalt(I) B12, Cobalt(Ii) B12, and Base-Off Adenosylcobalamin. *J. Am. Chem. Soc.* **1991**, *113*, 5299−5304.
(11) Barata, J. F. B.; Santos, C. I. M.; Neves, M. G. P. M. S.; Faustino, M. A. F.; Cavaleiro, J. A. S. Functionalization of Corroles. In *Synthesis and Modifications of Porphyrinoids*; Paolesse, R., Ed.; Springer Berlin Heidelberg: Berlin, Heidelberg, 2014; pp 79−141.
(12) Aviv, I.; Gross, Z. Corrole-Based Applications. *Chem. Commun.* **2007**, 1987−1999.
(13) Aviv-Harel, I.; Zeev, G. Aura of Corroles. *Chem. - Eur. J.* **2009**, *15*, 8382−8394.
(14) Gryko, D. T.; Fox, J. P.; Goldberg, D. P. Recent Advances in the Chemistry of Corroles and Core-Modified Corroles. *J. Porphyrins Phthalocyanines* **2004**, *08*, 1091−1105.
(15) Zagal, J.; Páez, M.; Tanaka, A. A.; dos Santos, J. R.; Linkous, C. A. Electrocatalytic Activity of Metal Phthalocyanines for Oxygen Reduction. *J. Electroanal. Chem.* **1992**, *339*, 13−30.
(16) Levy, N.; Mahammed, A.; Kosa, M.; Major, D. T.; Gross, Z.; Elbaz, L. Metallocorroles as Nonprecious-Metal Catalysts for Oxygen Reduction. *Angew. Chem., Int. Ed.* **2015**, *54*, 14080−14084.
(17) Friedman, A.; Landau, L.; Gonen, S.; Gross, Z.; Elbaz, L. Efficient Bio-Inspired Oxygen Reduction Electrocatalysis with Electropolymerized Cobalt Corroles. *ACS Catal.* **2018**, *8*, 5024−5031.
(18) Morozan, A.; Campidelli, S.; Filoramo, A.; Jousselme, B.; Palacin, S. Catalytic Activity of Cobalt and Iron Phthalocyanines or Porphyrins Supported on Different Carbon Nanotubes Towards Oxygen Reduction Reaction. *Carbon* **2011**, *49*, 4839−4847.
(19) Lai, W.; Cao, R.; Dong, G.; Shaik, S.; Yao, J.; Chen, H. Why Is Cobalt the Best Transition Metal in Transition-Metal Hangman Corroles for O−O Bond Formation During Water Oxidation? *J. Phys. Chem. Lett.* **2012**, *3*, 2315−2319.
(20) Levy, N.; Mahammed, A.; Friedman, A.; Gavriel, B.; Gross, Z.; Elbaz, L. Metallocorroles as Non-Precious Metal Electrocatalysts for Highly Efficient Oxygen Reduction in Alkaline Media. *ChemCatChem* **2016**, *8*, 2832−2837.
(21) Levy, N.; Shpilman, J. S.; Honig, H. C.; Major, D. T.; Elbaz, L. A Surprising Substituent Effect in Corroles on the Electrochemical Activation of Oxygen Reduction. *Chem. Commun.* **2017**, *53*, 12942−12945.
(22) Anastasijević, N. A.; Vesović, V.; Adžić, R. R. Determination of the Kinetic Parameters of the Oxygen Reduction Reaction Using the Rotating Ring-Disk Electrode: Part I. Theory. *J. Electroanal. Chem.* **1987**, *229*, 305−316.
(23) Kulkarni, A.; Siahrostami, S.; Patel, A.; Nørskov, J. K. Understanding Catalytic Activity Trends in the Oxygen Reduction Reaction. *Chem. Rev.* **2018**, *118*, 2302−2312.
(24) Orłowski, R.; Tasior, M.; Staszewska-Krajewska, O.; Dobrzycki, Ł.; Schilf, W.; Ventura, B.; Cyrański, M. K.; Gryko, D. T. Hydrogen Bonds Involving Cavity Nh Protons Drives Supramolecular Oligomerization of Amido-Corroles. *Chem. - Eur. J.* **2017**, *23*, 10195−10204.
(25) Levy, N.; Mahammed, A.; Kosa, M.; Major, D. T.; Gross, Z.; Elbaz, L. Metallocorroles as Nonprecious-Metal Catalysts for Oxygen Reduction. *Angew. Chem., Int. Ed.* **2015**, *54*, 14080−14084.
(26) Giannozzi, P.; et al. Quantum Espresso: A Modular and Open-Source Software Project for Quantum Simulations of Materials. *J. Phys.: Condens. Matter* **2009**, *21*, No. 395502.
(27) Perdew, J. P.; Burke, K.; Ernzerhof, M. Generalized Gradient Approximation Made Simple. *Phys. Rev. Lett.* **1996**, *77*, 3865−3868.
(28) Perdew, J. P.; Burke, K.; Ernzerhof, M. Generalized Gradient Approximation Made Simple [Phys. Rev. Lett. 77, 3865 (1996)]. *Phys. Rev. Lett.* **1997**, *78*, 1396.
(29) Garrity, K. F.; Bennett, J. W.; Rabe, K. M.; Vanderbilt, D. Pseudopotentials for High-Throughput Dft Calculations. *Comput. Mater. Sci.* **2014**, *81*, 446−452.
(30) Methfessel, M.; Paxton, A. T. High-Precision Sampling for Brillouin-Zone Integration in Metals. *Phys. Rev. B* **1989**, *40*, 3616−3621.
(31) Nørskov, J. K.; Rossmeisl, J.; Logadottir, A.; Lindqvist, L.; Kitchin, J. R.; Bligaard, T.; Jónsson, H. Origin of the Overpotential for Oxygen Reduction at a Fuel-Cell Cathode. *J. Phys. Chem. B* **2004**, *108*, 17886−17892.
(32) Koszarna, B.; Gryko, D. T. Efficient Synthesis of Meso-Substituted Corroles in a H2o−Meoh Mixture. *J. Org. Chem.* **2006**, *71*, 3707−3717.
(33) Kosa, M.; Levy, N.; Elbaz, L.; Major, D. T. Theoretical Study of the Electrocatalytic Reduction of Oxygen by Metallocorroles. *J. Phys. Chem. C* **2018**, *122*, 17686−17694.
(34) Levy, N.; Mahammed, A.; Friedman, A.; Gavriel, B.; Gross, Z.; Elbaz, L. Metallocorroles as Non-Precious Metal Electrocatalysts for Highly Efficient Oxygen Reduction in Alkaline Media. *ChemCatChem* **2016**, *8*, 2832−2837.
(35) Levy, N.; Mahammed, A.; Kosa, M.; Major, D. T.; Gross, Z.; Elbaz, L. Metallocorroles as Nonprecious-Metal Catalysts for Oxygen Reduction. *Angew. Chem.* **2015**, *127*, 14286−14290.
(36) Busch, M.; Fabrizio, A.; Luber, S.; Hutter, J.; Corminboeuf, C. Exploring the Limitation of Molecular Water Oxidation Catalysts. *J. Phys. Chem. C* **2018**, *122*, 12404−12412.
(37) Kosa, M.; Levy, N.; Elbaz, L.; Major, D. T. Theoretical Study of the Electrocatalytic Reduction of Oxygen by Metallocorroles. *J. Phys. Chem. C* **2018**, 17686.
(38) Noffke, B. W.; Li, Q.; Raghavachari, K.; Li, L. S. A Model for the Ph-Dependent Selectivity of the Oxygen Reduction Reaction Electrocatalyzed by N-Doped Graphitic Carbon. *J. Am. Chem. Soc.* **2016**, *138*, 13923−13929.

DOI: 10.1021/acs.jpcc.9b07333
J. Phys. Chem. C 2019, 123, 26351−26357